第51卷第6期 中国科学技术大学学报 Vol. 51, No. 6
2021年6月 JOURNAL OF UNIVERSITY OF SCIENCE AND TECHNOLOGY OF CHINA Jun. 2021
Received: 2021-03-21; Revised: 2021-04-10 doi:10.52396/JUST-2021-0084

Hydrogen activation over stoichiometric and defective CeO_2 surfaces: A first-principles study

CHEN Zihui[1], ZHAO Chuanlin[1], LIU Jinxun[1*], LI Weixue[1,2*]
1. Department of Chemical Physics, School of Chemistry and Materials Science, University of Science and Technology of China, Hefei 230026, China;
2. Hefei National Laboratory for Physical Sciences at the Microscale, University of Science and Technology of China, Hefei 230026, China
* Corresponding author. E-mail: jxliu86@ustc.edu.cn; wxli70@ustc.edu.cn

Abstract: Hydrogen activation plays a pivotal role in hydrogenation reactions over transition metal oxide catalysts. Clarifying hydrogen activation over ceria oxide (CeO_2) is an important issue in the acetylene hydrogenation reaction. Employing density functional theory (DFT) calculations, we studied hydrogen activation over stoichiometric and defective CeO_2 (111), (110), and (100) surfaces. Hydrogen dissociates on the stoichiometric CeO_2 surfaces only forming hydroxyl groups. The presence of oxygen vacancies can promote the H_2 activation over the defective CeO_2 surfaces. Both H^+ and H^- species can be found on the defective CeO_2(111) and (100) surfaces, whereas only H^+ species can be observed on the defective CeO_2(110) surface. The structure sensitivity of the H_2 activation over the stoichiometric and defective CeO_2 surfaces is correlated with H^+ and H^- adsorption energies determined by the ability of the surface oxygen vacancy formation and charge distributions of Ce and O ions. Our work provides more insight into H_2 activation on CeO_2-based catalysts which will guide better catalyst design for hydrogenation reactions.

Keywords: CeO_2; hydrogen activation; surface sensitivity; density functional theory
CLC number: O647.1 **Document code**: A

1 Introduction

Partial hydrogenation of alkynes to olefins is one of the most important industrial reactions and is widely used to purify olefin streams usually containing acetylenic[1]. One of the most commonly used catalysts in partial hydrogenation of alkynes to olefins is Pd which, however, shows a high tendency in excessive hydrogenation in the formation of alkanes and polymerization of alkynes. To tackle this issue, Pd metal alloying with other metals was synthesized to suppress the over-hydrogenation of alkynes[2-4]. For example, alloying Pd with a less active metal can weaken acetylene adsorption and destroy the formation of the β-hydride phase thus improving the selectivity of the partial hydrogenation reaction of alkynes toward olefins[3]. However, the high cost of Pd limits its scale-up application in the industry. To maximize the atom-utilization efficiency, a variety of single-atom catalysts have been synthesized to catalyze alkynes hydrogenation reaction[5]. Many works reported that Pt, Pd, Rh, and other transition metal single atoms deposited on graphene and black phosphorus show high catalytic activity in alkyne hydrogenation[6-8]. However, the single-atom catalysts are often difficult to prepare and ready to aggregate to form large nanoparticles in practice[5]. Therefore, it is highly desirable to design catalysts with high stability, activity, and selectivity for alkyne hydrogenation to replace the usage of expensive noble metal catalysts.

As a popular catalytic material, ceria oxide (CeO_2) is widely used as the support and catalyst[9-12] and applied to solid oxide fuel cells[13,14] and oxygen sensors[15,16], which is attributed to its low price[17], excellent acid-base properties, and redox properties[18]. Consequently, CeO_2 has gained much current interest in catalysis originating from its superior activity and selectivity for many chemical reactions including alkyne semi-hydrogenation reactions[19-23]. Pérez-Ramírez and coworkers[19] found the conversion of propyne and the selectivity of olefins can be achieved as high as 91% and 96% for propyne hydrogenation reaction over bulk CeO_2 catalyst at the reaction condition of T = 523 K and P = 1 bar with H_2/C_2H_2 ratio of 30:1,

Citation: CHEN Zihui, ZHAO Chuanlin, LIU Jinxun, et al. Hydrogen activation over stoichiometric and defective CeO_2 surfaces: A first-principles study. J. Univ. Sci. Tech. China, 2021, 51(6): 485-493.

respectively. Generally, CeO_2 displays better catalytic performance in acetylene hydrogenation as compared with conventional noble Pd-based catalysts[2,24]. Carrasco and coworkers[20] revealed that the hydrogen dissociation has the highest activation barrier and can be considered as the rate-determining step for acetylene hydrogenation over the CeO_2(111) surface. Consistent with this work, many groups[25,26] also demonstrated the difficulty of hydrogen activation in the hydrogenation of alkynes over the CeO_2(111) surface or bulks. Since H_2 activation plays an important role in the acetylene and/or alkynes hydrogenation reaction, the exploration of H_2 activation over the CeO_2 surfaces is pivotal to design better CeO_2-based catalysts for acetylene and/or alkynes hydrogenation.

Different from metals, there are generally two different routes for the H_2 dissociation over metal oxide surfaces, namely, homolytic and heterolytic dissociation of H_2. The homolytic H_2 dissociation often generates two OH groups over metal oxides that are difficult to be reduced, such as MgO[27,28], Al_2O_3 and SiO_2[29]. Whereas heterolytic H_2 dissociation generates an H cation bound to O anion and an H anion bound to the metal cation. Many experimental and theoretical works indicate that the heterolytic H_2 dissociation is more likely to occur over reducible oxides[30-32], such as CeO_2[33] and TiO_2[34]. Density functional theory (DFT) calculations reported that the homolytic H_2 dissociation is dominant on CeO_2(111)[20,30] with an activation barrier larger than 1 eV. Therefore, the H_2 dissociation is difficult on the CeO_2(111) surface at a relatively low temperature corroborated by the experimental measurements[19,20]. A similar high activation barrier of the H_2 dissociation was also found for the reverse methanol-reforming reaction over different kinds of CeO_2 surfaces[22].

In contrast to a well-defined CeO_2(111) surface, the heterolytic H_2 dissociation is more kinetically feasible over the reduced CeO_2(111) surfaces[1,35,36]. The presence of surface oxygen vacancies (Vo) on CeO_2 surfaces promotes the cleavage of hybrid H−H bonds and increases the catalytic activity of alkyne hydrogenation[1,35]. Ramirez-Cuesta et al.[37] gave the first direct evidence for the presence of both surfaces and bulk Ce−H species on partially reduced ceria rods via in situ inelastic neutron scattering spectroscopy. A new heterolytic H_2 dissociation mechanism was proposed by Huang et al.[36] that the dissociated H species might be bound to Ce^{3+}_{Vo} sites in the form of hydrides over the reduced CeO_{2-x}(111) thin films and CeO_{2-x} powders at room temperature. Therefore, heterolytic H_2 dissociation forming H anion species binding Ce cation is feasible over the reduced CeO_2(111) surface. Besides the oxygen vacancy effect on the H_2 activation, many studies demonstrated the reactivities of H_2 activation and acetylene hydrogenation reactions are often surface orientation dependent on CeO_2 catalysts[38-40]. For example, it was found that C_2H_2 hydrogenation reaction prefers to occur on polyhedral CeO_2 particles, whereas the CO oxidation reaction tends to take place over CeO_2 nanocubes and nanorods[39]. Calatayud and coworkers[40] have investigated seven different CeO_2 terminations displaying distinct activities in the hydrogen activation, which indicates the strong structure sensitivity of the H_2 activation over CeO_2-based catalysts.

Although many investigations are done, there are still open on whether and why the oxygen vacancy can promote hydrogenation activation over CeO_2 catalyst and how the different stoichiometric and defective surfaces of CeO_2 impact H_2 activation. In the present work, we studied H_2 activation over the stoichiometric and defective (111), (110), and (100) facets of CeO_2. The structure sensitivity of the H_2 activation and oxygen vacancy effect on H_2 activation are revealed on CeO_2. The most probable H species on the stoichiometric and defective CeO_2 surfaces are identified. Our work provides more insight into the H_2 activation over the CeO_2 based catalyst which guides a better CeO_2-based catalyst design for acetylene hydrogenation reactions.

2 Computational methods

Spin-polarized periodic density functional theory (DFT) calculations were performed by using the Vienna ab initio simulation package (VASP)[41,42]. The exchange-correlation potential was treated by the generalized gradient approximation (GGA) in the Perdew-Burke-Ernzerh (PBE) functional form[43]. The projected-augmented wave (PAW) pseudopotentials were utilized to describe the core electrons[44], and the Kohn-Sham valence states were expanded in a plane-wave basis set with the kinetic energy of 400 eV. The Brillouin zone integration was sampled with 12×12×12 Monkhorst-Pack mesh k-points for the bulk CeO_2 calculations. The equilibrium lattice constant for bulk CeO_2 was optimized to be 5.45 Å, in good agreement with the experimental measurement of 5.41 Å[45]. The DFT + U methodology was used to treat the on-site Coulomb and the exchange interaction of the strongly localized Ce 4f electrons with an effective U_{eff} = 5 eV. Here, we adopted U values of 2 eV and 5 eV, which represent a low U value and a high U value respectively, to calculate hydrogen dissociation energies on defective CeO_2(111) surfaces (Table S1). The difference in H_2 dissociative

adsorption energies by using a low and a high U values are 0.29 eV and 1.33 eV forming H^+/H^- and H^+/H^+, respectively. Different U values will result in significantly different H_2 dissociative adsorption energies. Hydrogen dissociation on the CeO_{2-x}(111) surface is more difficult by using a low U value which conflicts with the experiment results[1,36,37] that oxygen vacancy can promote hydrogen activation. However, a high U value of 5 eV is considered to provide localization of the electrons left upon oxygen removal from CeO_2[46]. Therefore, we used the U value of 5 eV for the surface adsorption and reaction calculations in the present work.

The O-terminated CeO_2(111) surface with a (2×2) unit cell, a Tasker Type 2 surface[47], was modeled by a four-layers slab with the bottom two layers fixed at their bulk positions (Figure 1(a)). The CeO_2(110) with a (2×2) unit cell, a Tasker Type 1 surface[47], was modeled by a periodic five-layers slab with the bottom two layers fixed at their bulk positions (Figure 1(b)). Whereas the O-terminated CeO_2(100) with (3x3) periodicity, a Tasker Type 3 surface[47], was modeled by a periodic seven-layer slab with the bottom two layers fixed at their bulk positions (Figure 1(c)). To eliminate the dipole moment perpendicular to the CeO_2(100) surface[23], half of the O atoms from the top layer are removed, which has been commonly applied in many previous computational studies[48,49].

A 3×3×1 Monkhorst-Pack mesh k-points were used for calculations of H_2 activations over three different CeO_2 surfaces. All slabs were separated by a 12 Å vacuum. All structures were relaxed until forces on each ion were less than 0.02 eV/Å, and the convergence criterion for energy was 10^{-4} eV. Transition structures (TS) for the considered reaction paths were located by using the climbing-image nudged elastic band (CI-NEB) algorithm. The adsorption energy was calculated as $E_{ads} = E_{total} - E_{slab} - E_{gas}$, where E_{total}, E_{slab}, and E_{gas} refer to the energy of the slab with adsorbate, the energy of clean CeO_2 surfaces, and the energy of a gas-phase molecule in a neutral state, respectively. the H_2 activation barrier is calculated as the energy difference between the transition state and the adsorption state of H_2 over CeO_2 surfaces.

3 Results

3.1 Structure sensitivity of H_2 activation over stoichiometric CeO_2 surfaces

We studied H_2 activation over the three low-index facets of CeO_2(Figure 1), namely (111), (110), and (100) surfaces, which are prototypical examples of three types of ionic crystal facets. The O and Ce atoms are distributed alternately over the O-terminated CeO_2(111) surface, where the surface O atom is coordinated with three Ce atoms and each Ce atom binds three O atoms. Similarly, O and Ce atoms are distributed alternately on the O-terminated CeO_2(100) surface, whereas surface O atoms are coordinated with three Ce atoms but each Ce atom binds two surfaces and four lattice oxygen atoms. The O and Ce atoms are distributed in the same layer on the CeO_2(110) surface, in which the surface O atom binds two Ce atom and Ce atoms are coordinated with four surface and two lattice oxygen atoms. The different surface structures of CeO_2(111), (110), and (100) surfaces will exhibit the distinct catalytic performance of H_2 activation. H_2 first adsorbs on the CeO_2 surface and then heterolytic dissociate in the formation of an H^+ bound to the O anion and an H^- bound to the Ce cation (Figure 2). When H atom adsorbs at the O anion site, more electrons can transfer from H to O forming H cation due to the higher electronegativity of O as compared with H. The Bader charges of H atoms at the Ce cation and O anion site are −0.17, −0.15, −0.66 and +0.17, −0.09, +0.21 over CeO_2(111), (110), and (100) surfaces, respectively (Table S2). Later, the dissociated H atom migrates from the Ce cation to the O anion site. The calculated potential energy surface diagrams and corresponding configures for H_2 activation are shown in Figure 3.

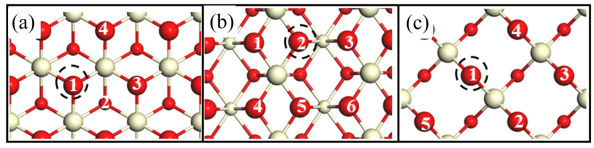

Figure 1. The top view of CeO_2(111) (a), CeO_2(110) (b) and CeO_2(100) (c) surfaces. Red and beige spheres are the O and Ce atoms, respectively. Small spheres stand for the subsurface O and Ce atoms. The dashed black circles represent the oxygen vacancies. This notation is used throughout this paper. The indicated numbers are non-equivalent oxygen atoms.

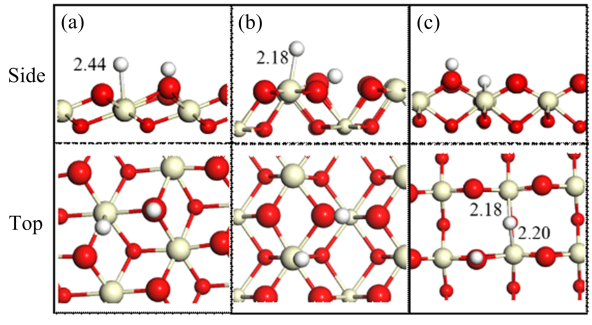

Figure 2. Top and side views of optimized configurations for heterolytic H_2 dissociative adsorption over stoichiometric CeO_2 (111) (a), CeO_2(110) (b), and CeO_2(100) (c) surfaces. The H−Ce bond distances are indicated in Å.

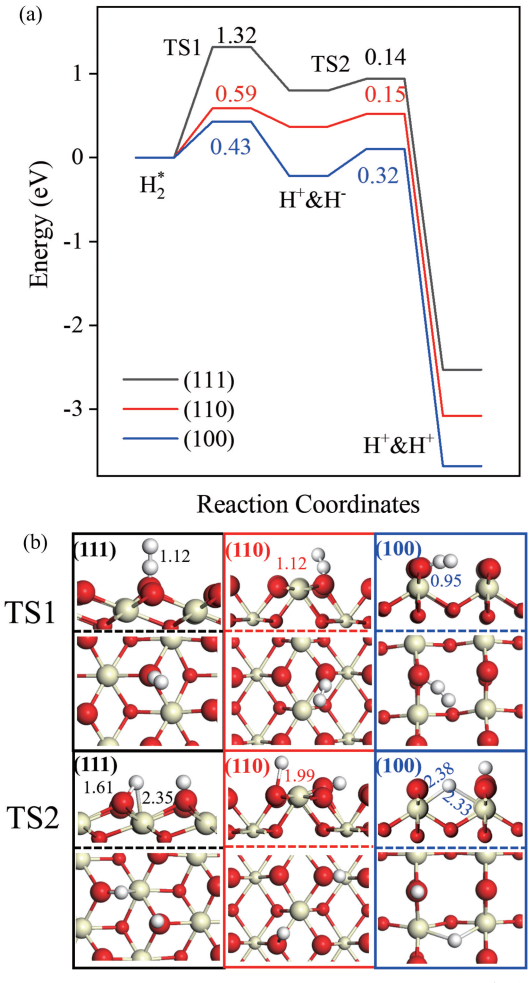

Figure 3. The potential energy surface diagram (a) and corresponding transition state configurations (b) for heterolytic H_2 dissociation over the stoichiometric CeO_2(111), (110), and (100) surfaces. The bond distance between the two dissociated H atoms is indicated in Å.

There is a weak interaction between the H_2 and stoichiometric CeO_2 surfaces and H_2 physically adsorbs on the stoichiometric CeO_2 surfaces with the adsorption energies higher than −0.10 eV. Two different H_2 dissociation mechanisms, namely the heterolytic and homolytic dissociation of H_2, are considered in the present work. The bond distance of two surface neighboring oxygen atoms in CeO_2 surfaces is larger than 3.85 Å, which is longer than that of the Ce−O bond, the heterolytic H_2 dissociation has a high priority to occur. the limiting distance for hemolytic H_2 dissociation to occur is determined by the distance between neighboring surface O atoms. Therefore, we studied the heterolytic dissociation of H_2 at the Ce−O pair (Figure 2), and then the adsorbed H^+ at the Ce cation site might migrate to the O anion thus forming the homolytic H_2 dissociative adsorption modes on CeO_2 surfaces.

The heterolytic dissociation of H_2 is sensitive to the surface structure of CeO_2 from both thermodynamic and kinetic aspects. Specifically, the heterolytic dissociation of H_2 to generate an H^+ and an H^- is endothermic by 0.80 eV with an activation barrier of 1.32 eV over the CeO_2(111) surface. The high energy cost and activation barrier require a relatively high reaction temperature for the heterolytic dissociation of H_2 on CeO_2(111). As shown in Table S3 and Figure S1, we can see H binding strength increases with the Ce−H bond length increasing from 2.2 to 2.5 Å where a chemical bond can be formed between Ce and H. However, H binding energy becomes +2.2 eV when the bond distance between H and Ce is larger than 2.6 Å indicating the physisorption of the H atom at the Ce cation site. As a result, the formed H anion at the Ce cation is ready to migrate to the neighboring O atom with a low activation barrier of 0.14 eV on the CeO_2(111) surface. Therefore, only H^+ can be found once H_2 dissociates on the CeO_2(111) surface.

Heterolytic dissociation of H_2 is more feasible on CeO_2(110) as compared with that on CeO_2(111) surface (Figure 3). The calculated reaction energy and activation barrier for the heterolytic dissociation of H_2 is moderate over the CeO_2(110) surface with the values of 0.37 eV and 0.59 eV, respectively. The activation barriers for the recombination of H^- and H^+ in the formation of H_2 and the migration of H^- from the Ce cation to the O anion are comparable over CeO_2(110) surface with the values of 0.22 and 0.15 eV, respectively. Therefore, one can observe abundant H^+ on the CeO_2(110) surface with rare H^- anions adsorption at the Ce cation site. Especially on the CeO_2(110) surface, some O anions can coordinate with two Ce^{3+}. The Bader charge of this kind of the O anion is high that fewer electrons can be exchanged with H. That's why the charge of the H ions binding with the O anion is zero or even negative (Table S2).

The heterolytic dissociation of H_2 is most feasible on the CeO_2(100) surface with the lowest activation barrier of 0.43 eV among the three considered CeO_2 surfaces due to the highly exothermic nature of the H_2 dissociation over the CeO_2(100) surface ($\Delta H = -0.22$ eV). After, H anion adsorbed at the Ce cation site can diffuse to the O anion site exothermically with a low activation barrier of 0.32 eV. Therefore, only H^+ can be found on the CeO_2(100) surface which has similar catalytic behavior but more active than the CeO_2(111) surface at relatively high temperatures. Our DFT calculations clearly revealed the difficulty of H_2 activation on the CeO_2(111) surface but much feasible on the open CeO_2(110) and (100) surfaces. Our result

is in line with other theoretical and experimental works that the H_2 dissociation is difficult on the stoichiometric CeO_2(111) surface[20,22,40,50]. A large number of stable hydroxyl groups can be generated on the three different stoichiometric CeO_2 surfaces for the H_2 activation. Therefore, a high reaction temperature is required for the hydrogenation of alkynes by the usage of H cation as the hydrogen resources. The hydrogen-to-acetylene ratio is usually larger than 20 that a large number of H_2 molecules can be activated providing enough H^+ species used for acetylene hydrogenation reactions[19,20].

3.2 Structure sensitivity of H_2 activation over defective CeO_2 surfaces

Oxygen vacancies often present on the CeO_2 surface inevitably under the acetylene hydrogenation reaction conditions. We studied the heterolytic H_2 dissociation mechanism over defective CeO_2 (111), (110), and (100) surfaces to reveal the oxygen vacancy effect on H_2 dissociation activity and corresponding surface H^+/H^- species distributions. The oxygen vacancy concentrations are different over (111), (110), and (100) surfaces with the values of 25% and 12.5%, 11.1%, respectively. The corresponding concentrations of Ce^{3+} over the three surfaces are around 12.5% to 8.3%, which are similar to the reduced CeO_2 materials prepared in experiments[36,51-53] with the Ce^{3+} concentration of 10% to 15%. The calculated optimal potential energy diagram for heterolytic H_2 dissociation and corresponding transition state configurations over the three defective CeO_2 surfaces are shown in Figure 4. The configurations of heterolytic dissociative of H_2 and corresponding structural information are shown in Figure S2 and Table S4, respectively. Similar to stoichiometric CeO_2 surfaces, H_2 still adsorbs weakly on the three considered defective CeO_2 surfaces with the adsorption energies of ~ −0.10 eV. However, the heterolytic H_2 dissociation is accelerated by the introduction of oxygen vacancies in CeO_2 surfaces from both thermodynamic and kinetic aspects (Figure 4). From the thermodynamic data in Table S4, we can see that on the defective CeO_{2-x}(111), (110), and (100) surfaces, H^- prefers to adsorb at the oxygen vacancy site, whereas H^+ prefer to bound with the surface oxygen atoms rather than subsurface oxygen atoms (Figure S2). For the defective CeO_{2-x} (111) surface, the heterolytic H_2 dissociative adsorption energy is −0.92 eV, which is much lower than that on the stoichiometric CeO_2(111) surface by 1.73 eV. As compared with stoichiometric CeO_2(110) and (100) surfaces, the defective surfaces have lower heterolytic H_2 dissociative adsorption energies of −0.67 eV and −0.68 eV, which are lower than those on the stoichiometric surfaces by 0.98 eV and

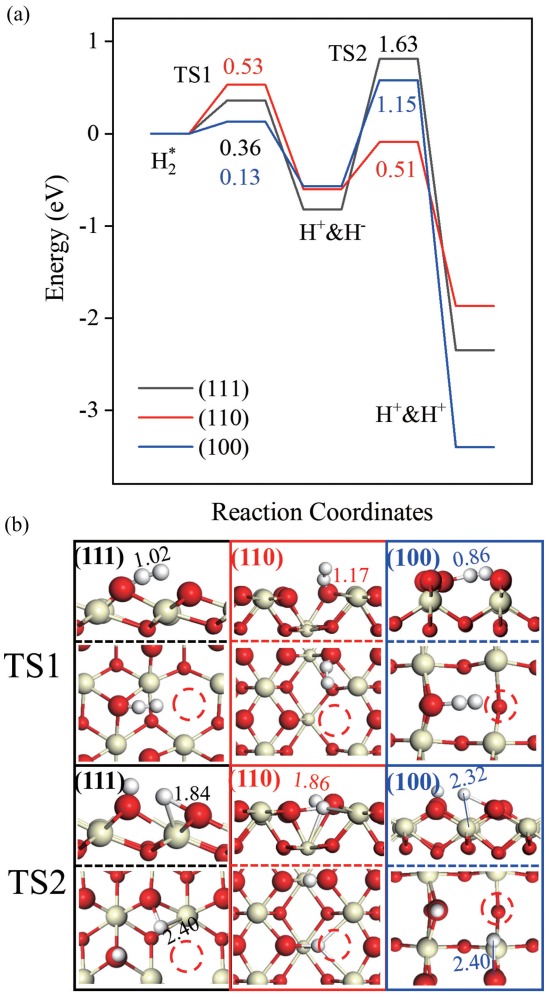

Figure 4. Potential energy surface diagram (a) and corresponding transition state configurations (b) for the heterolytic H_2 dissociation over the defective CeO_2 (111), (110), and (100) surfaces. The bond distances between the two dissociated H atoms are indicated in Å. Dashed red circles representing oxygen vacancies.

0.34 eV, respectively. Heterolytic H_2 dissociation is structure sensitive and the presence of oxygen vacancy can enhance the heterolytic H_2 dissociation thermodynamically.

The activation barrier of heterolytic H_2 dissociation forming H^+ and H^- species is reduced by the introduction of oxygen vacancy in CeO_2(111), (110), and (100) surfaces by 0.79, 0.23, and 0.30 eV, respectively. Therefore, the heterolytic H_2 dissociation can be accelerated on the defective CeO_2 surfaces as compared with the stoichiometric ones. However, H^- adsorption at the Ce cation site migrates to the O anion nearby has higher or comparable reaction barriers on the defective CeO_2(111), (110), and (100) surfaces as compared with those on the perfective ones by 1.49, −0.01, and 0.83 eV, respectively. This can be attributed to the less exothermic nature of the

hydrogenation migration with the introduction of oxygen vacancy in stoichiometric CeO_2 surfaces.

Different from the observations of merely H^+ on the three stoichiometric CeO_2 surfaces, H^+ and H^- can be found at a low temperature on the partially reduced CeO_{2-x}(111) and CeO_{2-x}(100) surfaces due to the higher activation barriers for H^- at the Ce cation site migration to O anion site forming H^+ species of 1.63 and 1.15 eV, respectively. The heterolytic H_2 dissociation and H^- migration from Ce to O forming H^+ have similar activation barriers of 0.53 and 0.51 eV over CeO_{2-x}(110) surface, respectively. However, the potential energy surface goes down for H_2 dissociation forming two H^+ species with low activation barriers that only H^+ species can be found on the defective CeO_2 (110) surface. The different catalytic behaviors of the H_2 dissociation between (110) and (111)/(100) surfaces can be attributed to the different bond strength of H^+/ H^- on defective CeO_2 surfaces.

As stated above, the heterolytic H_2 dissociation is sensitive to the surface structures of CeO_2 and oxygen vacancy plays an important role in the heterolytic dissociation of H_2 and migration of H atom from the Ce cation site to the O anion site. This can be originated from different oxygen vacancy formation energies over different stoichiometric CeO_2 surfaces. The defective CeO_2 surfaces have higher activities for the heterolytic H_2 dissociation than H species migration from the Ce cation to the O anion except for the perfect and defective CeO_2(110) surface sharing almost the same activities on the H migration. As a result, the surface stably adsorbed H species vary greatly over different stoichiometric and defective CeO_2 surfaces that only H^+ can be found on perfect CeO_2 surfaces and defective CeO_2(110) surface but both H^+ and H^- can be observed on the defective (111) and (100) surfaces. The different forms of H species might display distinct catalytic behaviors for acetylene hydrogenation reactions.

To further reveal the reason for the surface sensitivity of the H_2 dissociation, we calculated the binding energies of H^+ and H^- on stoichiometric and defective CeO_2 surfaces. In Figure S3, the sum of the isolated adsorption energies of H^+ and H^- is close to the coadsorption energy of the H^+ & H^- configuration. Therefore, there is no obvious interaction between the two H^+ and H^- ions due to the long distance between them for the coadsorption of H^+ & H^- species. By carefully evaluating the calculated H^+ & H^- binding energies and oxygen vacancy formation energies, we find a linear scaling relationships between H^+/H^- binding energies and oxygen vacancy formation energies

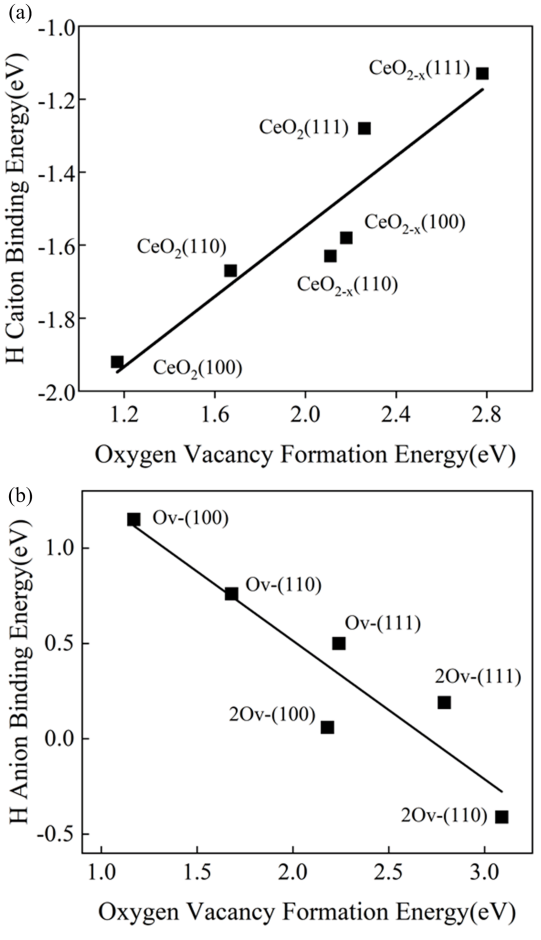

Figure 5. The linear scaling relationship between H^+(a)/H^-(b) binding energy and oxygen vacancy formation energy on the three reduced CeO_{2-x} surfaces.

(Figure 5). Generally, the binding strength of H^+ bounded to the O anion decreases by increasing the oxygen vacancy formation energy. The calculated oxygen vacancy formation energies on (111), (110), and (100) are 2.26, 1.67, and 1.17 eV, and the corresponding Bader charge state of O over the three surfaces are −1.09, −0.98, and −0.92, respectively. The stronger interaction between Ce and O will result in a larger Bader charge state of O cation weakening H^+ adsorption. The same observations can be found on the defective CeO_2 surfaces (Table S5). The surface sensitivity of homolytic adsorption is strongly correlated with the binding energy of H^+, which is determined by the ability of oxygen vacancy formation dependent on the CeO_2 surfaces. We further calculated hydrogen adsorption over the reduced CeO_{2-x} surfaces with two oxygen vacancies with the concentration of Ce^{3+} of 25% to 16.6%. The relationship established between the H adsorption energy and the oxygen vacancy formation energy is still valid and universal even considering high Ce^{3+} concentrations in the slab models (Figure S4).

H^- adsorption strength has an opposite trend as a function of the oxygen vacancy formation energies (Figure 5(b)). Generally, the harder the surface is to be reduced, the stronger bond can be formed between the Ce cation and the H anion. Compared with perfect surfaces, the Bader charge states of Ce cations over the defective CeO_2(111), (110), and (100) surfaces are also reduced to +1.01, +1.91, +2.15, respectively. The weaker charge state of Ce adsorbs H^- stronger at the Ce cation site due to the formation of the stronger covalent bond between H and Ce. This finding can be observed over the defective CeO_2 surfaces with two oxygen vacancies. As shown in Figure S5, it is found that there is no obvious relationship between the hydrogen activation barrier and oxygen vacancy formation energy. Due to the oxygen vacancies on the defective CeO_2 surface, the energy barrier for hydrogen dissociation is significantly reduced, and the surface is also more difficult to be further reduced. If the data is not classified, it does not comply with the law that the higher the oxygen vacancy formation energy, the higher the dissociation energy barrier. If discussed separately, it can be seen that the activation barriers for hydrogen activation are closely related to oxygen vacancy formation energy, that is, the higher oxygen vacancy formation energy, the higher hydrogen activation barrier on the stoichiometric and defective CeO_2 surfaces.

4 Conclusions

In the present work, we studied H_2 activation over the stoichiometric and defective CeO_2(111), (110), and (100) surfaces. The heterolytic H_2 dissociation pathway is dominant on stoichiometric and defective CeO_2 surfaces. We identified that the heterolytic H_2 dissociation is difficult on the stoichiometric CeO_2(111) surface corroborated by previous experimental measurements. CeO_2(100) and (110) surfaces are more active than (111) surfaces for the heterolytic H_2 dissociation. Only the H^+ adsorption at the O anions can be found on all three stoichiometric CeO_2 surfaces. The presence of oxygen vacancies can promote the heterolytic H_2 dissociation over defective CeO_2 surfaces. Both H^+ and H^- can be found on the defective CeO_2 (111) and (100) surfaces, whereas only H^+ species can be found on the CeO_2 (110) surface. The oxygen vacancy formation energy can be considered as a key descriptor for the activity of the heterolytic H_2 dissociation and the distribution of H^+/H^- species. Our work provides more insight into H_2 activation on CeO_2-based catalysts, which is pivotal for better catalyst design.

Supplementary data

Supplementary data are available at J. Univ. Sci. Tech. China online.

Acknowledgments

This work was supported by the Key Technologies R&D Program of China (2017YFB0602205, 2018YFA0208603), the National Natural Science Foundation of China (91945302), the Chinese Academy of Sciences Key Project (QYZDJ-SSW-SLH054), the start-up funds of University of Science and Technology of China (KY2060000171), USTC Research Funds of the Double First-Class Initiative (YD2060002012) and high-performance computational resources provided by University of Science and Technology of China (http://scc.ustc.edu.cn).

Conflict of interest

The authors declare no conflict of interest.

Author information

CHEN Zihui is currently a graduate student in the Department of Chemical Physics, School of Chemistry and Materials Science under the supervision of Prof. Li Weixue at University of Science and Technology of China. Her research mainly focuses on hydrogen activation on oxides surfaces.

LIU Jinxun (corresponding author) is currently working as a research fellow at the School of Chemistry and Materials Science, University of Science and Technology of China. He received his PhD from Dalian Institute of Chemical Physics and was a postdoctoral fellow in the Department of Chemical Engineering and Chemistry, Eindhoven University of Technology and in the Department of Chemical Engineering, University of Michigan-Ann Arbor. His research expertise spans computational heterogeneous catalysis, electrocatalysis, machine learning, and molecular simulation.

LI Weixue (corresponding author) received his PhD from the Chinese Academy of Sciences in 1998. He did his postdoctoral research at Fritz Haber Institut der MPG and University of Aarhus from 1999 to 2004. He joined the Dalian Institute of Chemical Physics and led the "Theoretical Catalysis Group" at the State Key Laboratory of Catalysis from 2004 to 2015. Since 2015, he is the Professor of Chemistry at University of Science and Technology of China. His research focuses on the computational and AI investigation of heterogeneous catalysis, particularly on the hydrocarbon conversion and design of the ultrastable nanocatalysts.

References

[1] Riley C, Zhou S, Kunwar D, et al. Design of effective catalysts for selective alkyne hydrogenation by doping of ceria with a single-atom promotor. Journal of the American Chemical Society, 2018, 140(40): 12964−12973.

[2] Teschner D, Borsodi J, Wootsch A, et al. The roles of subsurface carbon and hydrogen in palladium-catalyzed alkyne hydrogenation. Science, 2008, 320(5872): 86−89.

[3] Studt F, Abild-Pedersen F, Bligaard T, et al. Identification of non-precious metal alloy catalysts for selective hydrogenation of acetylene. Science, 2008, 320 (5881): 1320.
[4] Khan N A, Shaikhutdinov S, Freund H J. Acetylene and ethylene hydrogenation on alumina supported Pd-Ag model catalysts. Catalysis Letters, 2006, 108 (3): 159-164.
[5] Hannagan R T, Giannakakis G, Flytzani-Stephanopoulos M, et al. Single-atom alloy catalysis. Chemical Reviews, 2020, 120 (21): 12044-12088.
[6] Huang F, Deng Y, Chen Y, et al. Atomically dispersed Pd on nanodiamond/graphene hybrid for selective hydrogenation of acetylene. Journal of the American Chemical Society, 2018, 140 (41): 13142-13146.
[7] Zhuo H Y, Yu X, Yu Q, et al. Selective hydrogenation of acetylene on graphene-supported non-noble metal single-atom catalysts. Science China Materials, 2020, 63 (9): 1741-1749.
[8] Vanni M, Serrano-Ruiz M, Telesio F, et al. Black phosphorus/palladium nanohybrid: Unraveling the nature of P-Pd interaction and application in selective hydrogenation. Chemistry of Materials, 2019, 31 (14): 5075-5080.
[9] Farnesi Camellone M, Negreiros Ribeiro F, Szabová L, et al. Catalytic proton dynamics at the water/solid interface of ceria-supported Pt clusters. Journal of the American Chemical Society, 2016, 138 (36): 11560-11567.
[10] Ye X, Wang H, Lin Y, et al. Insight of the stability and activity of platinum single atoms on ceria. Nano Research, 2019, 12 (6): 1401-1409.
[11] Parastaev A, Muravev V, Osta E, et al. Boosting CO_2 hydrogenation via size-dependent metal-support interactions in cobalt/ceria-based catalysts. Nature Catalysis, 2020, 3: 526-533.
[12] Kašpar J, Fornasiero P, Graziani M. Use of CeO_2-based oxides in the three-way catalysis. Catalysis Today, 1999, 50 (2): 285-298.
[13] Eguchi K, Setoguchi T, Inoue T, et al. Electrical properties of ceria-based oxides and their application to solid oxide fuel cells. Solid State Ionics, 1992, 52 (1): 165-172.
[14] Liu Z, Ding D, Liu M, et al. High-performance, ceria-based solid oxide fuel cells fabricated at low temperatures. Journal of Power Sources, 2013, 241: 454-459.
[15] Rajabbeigi N, Elyassi B, Khodadadi A, et al. A novel miniaturized oxygen sensor with solid-state ceria-zirconia reference. Sensors and Actuators B: Chemical, 2004, 100 (1): 139-142.
[16] Izu N, Shin W, Matsubara I, et al. Development of resistive oxygen sensors based on cerium oxide thick film. Journal of Electroceramics, 2004, 13 (1): 703-706.
[17] Montini T, Melchionna M, Monai M, et al. Fundamentals and catalytic applications of CeO_2-based materials. Chemical Reviews, 2016, 116 (10): 5987-6041.
[18] Paier J, Penschke C, Sauer J. Oxygen defects and surface chemistry of ceria: Quantum chemical studies compared to experiment. Chemical Reviews, 2013, 113 (6): 3949-3985.
[19] Vilé G, Bridier B, Wichert J, et al. Ceria in hydrogenation catalysis: High selectivity in the conversion of alkynes to olefins. Angewandte Chemie International Edition, 2012, 51 (34): 8620-8623.
[20] Carrasco J, Vilé G, Fernández-Torre D, et al. Molecular-level understanding of CeO_2 as a catalyst for partial alkyne hydrogenation. The Journal of Physical Chemistry C, 2014, 118 (10): 5352-5360.
[21] Vilé G, Colussi S, Krumeich F, et al. Opposite face sensitivity of CeO_2 in hydrogenation and oxidation catalysis. Angewandte Chemie International Edition, 2014, 53 (45): 12069-12072.
[22] Capdevila-Cortada M, García-Melchor M, López N. Unraveling the structure sensitivity in methanol conversion on CeO_2: A DFT+U study. Journal of Catalysis, 2015, 327: 58-64.
[23] Mullins D R. The surface chemistry of cerium oxide. Surface Science Reports, 2015, 70 (1): 42-85.
[24] García-Mota M, Gómez-Díaz J, Novell-Leruth G, et al. A density functional theory study of the 'mythic' Lindlar hydrogenation catalyst. Theoretical Chemistry Accounts, 2011, 128 (4): 663-673.
[25] Vilé G, Dähler P, Vecchietti J, et al. Promoted ceria catalysts for alkyne semi-hydrogenation. Journal of Catalysis, 2015, 324: 69-78.
[26] Ganduglia-Pirovano M V, Popa C, Sauer J, et al. Role of ceria in oxidative dehydrogenation on supported vanadia catalysts. Journal of the American Chemical Society, 2010, 132 (7): 2345-2349.
[27] da Silva Alvim R, Borges I, Leitão A A. Proton migration on perfect, vacant, and doped MgO(001) surfaces: Role of dissociation residual groups. The Journal of Physical Chemistry C, 2018, 122 (38): 21841-21853.
[28] Chen H Y T, Giordano L, Pacchioni G. From heterolytic to homolytic H_2 dissociation on nanostructured MgO(001) films as a function of the metal support. The Journal of Physical Chemistry C, 2013, 117 (20): 10623-10629.
[29] Martin D, Duprez D. Mobility of surface species on oxides. 1. Isotopic exchange of $^{18}O_2$ with ^{16}O of SiO_2, Al_2O_3, ZrO_2, MgO, CeO_2, and CeO_2-Al_2O_3. Activation by noble metals. Correlation with oxide basicity. The Journal of Physical Chemistry, 1996, 100 (22): 9429-9438.
[30] García-Melchor M, López N. Homolytic products from heterolytic paths in H_2 dissociation on metal oxides: The example of CeO_2. The Journal of Physical Chemistry C, 2014, 118 (20): 10921-10926.
[31] Syzgantseva O, Calatayud M, Minot C. Hydrogen adsorption on monoclinic $(\bar{1}11)$ and $(\bar{1}01)$ ZrO_2 surfaces: A periodic ab initio study. The Journal of Physical Chemistry C, 2010, 114 (27): 11918-11923.
[32] Wu Z, Zhang W, Xiong F, et al. Active hydrogen species on TiO_2 for photocatalytic H_2 production. Physical Chemistry Chemical Physics, 2014, 16 (15): 7051-7057.
[33] Schweke D, Shelly L, Ben David R, et al. A comprehensive study of the ceria-H_2 system: Effect of the reaction conditions on the reduction extent and intermediates. The Journal of Physical Chemistry C, 2020, 124 (11): 6180-6187.
[34] Menetrey M, Markovits A, Minot C. Reactivity of a reduced metal oxide surface: Hydrogen, water and carbon monoxide adsorption on oxygen defective rutile TiO_2(110). Surface Science, 2003, 524 (1): 49-62.

[35] Huang Z Q, Liu L P, Qi S, et al. Understanding all-solid frustrated Lewis pair sites on CeO_2 from theoretical perspectives. ACS Catalysis, 2018, 8 (1): 546-554.
[36] Li Z, Werner K, Qian K, et al. Oxidation of reduced ceria by incorporation of hydrogen. Angewandte Chemie International Edition, 2019, 58 (41): 14686-14693.
[37] Wu Z, Cheng Y, Tao F, et al. Direct neutron spectroscopy observation of cerium hydride species on a cerium oxide catalyst. Journal of the American Chemical Society, 2017, 139 (28): 9721-9727.
[38] Cao T, You R, Li Z, et al. Morphology-dependent CeO_2 catalysis in acetylene semihydrogenation reaction. Applied Surface Science, 2020, 501: 144120.
[39] Vilé G, Colussi S, Krumeich F, et al. Opposite face sensitivity of CeO_2 in hydrogenation and oxidation catalysis. Angewandte Chemie International Edition, 2014, 53 (45): 12069-12072.
[40] Matz O, Calatayud M. Breaking H_2 with CeO_2: Effect of surface termination. ACS Omega, 2018, 3 (11): 16063-16073.
[41] Kresse G, Hafner J. Ab initio molecular dynamics for liquid metals. Physical Review B, 1993, 47 (1): 558-561.
[42] Kresse G, Furthmüller J. Efficient iterative schemes for ab initio total-energy calculations using a plane-wave basis set. Physical Review B, 1996, 54 (16): 11169-11186.
[43] Perdew J P, Burke K, Ernzerhof M. Generalized gradient approximation made simple [Phys. Rev. Lett. 77, 3865 (1996)]. Physical Review Letters, 1997, 78 (7): 1396.
[44] Kresse G, Joubert D. From ultrasoft pseudopotentials to the projector augmented-wave method. Physical Review B, 1999, 59: 1758.
[45] Kümmerle E A, Heger G. The structures of C-$Ce_2O_{3+\delta}$, Ce_7O_{12}, and $Ce_{11}O_{20}$. Journal of Solid State Chemistry, 1999, 147 (2): 485-500.
[46] Castleton C W, Kullgren J, Hermansson K. Tuning LDA+U for electron localization and structure at oxygen vacancies in ceria. The Journal of Chemical Physics, 2007, 127 (24): 244704.
[47] Tasker P W. The stability of ionic crystal surfaces. Journal of Physics C: Solid State Physics, 1979, 12 (22): 4977-4984.
[48] Zhou C Y, Wang D, Gong X Q. A DFT+U revisit of reconstructed CeO_2 (100) surfaces: Structures, thermostabilities and reactivities. Physical Chemistry Chemical Physics, 2019, 21 (36): 19987-19994.
[49] Kim Y, Lee H, Kwak J H. Mechanism of CO oxidation on Pd/CeO_2 (100): The unique surface-structure of CeO_2 (100) and the role of peroxide. ChemCatChem, 2020, 12 (20): 5164-5172.
[50] Chen H T, Choi Y M, Liu M, et al. A theoretical study of surface reduction mechanisms of CeO_2(111) and (110) by H_2. ChemPhysChem, 2007, 8 (6): 849-855.
[51] Li Z, Werner K, Chen L, et al. Interaction of hydrogen with ceria: Hydroxylation, reduction, and hydride formation on the surface and in the bulk. Chemistry, 2021, 27 (16): 5268-5276.
[52] Özkan E, Cop P, Benfer F, et al. Rational synthesis concept for cerium oxide nanoparticles: On the impact of particle size on the oxygen storage capacity. The Journal of Physical Chemistry C, 2020, 124 (16): 8736-8748.
[53] Dutta P, Pal S, Seehra M S, et al. Concentration of Ce^{3+} and oxygen vacancies in cerium oxide nanoparticles. Chemistry of Materials, 2006, 18 (21): 5144-5146.

基于第一性原理的二氧化铈完整和缺陷表面上氢气活化研究

陈姊慧[1],赵川林[1],刘进勋[1*],李微雪[1,2*]
1. 中国科学技术大学化学与材料科学学院化学物理系,安徽合肥 230026;
2. 中国科学技术大学合肥微尺度物质科学国家研究中心,安徽合肥 230026
* 通讯作者. E-mail: jxliu86@ustc.edu.cn; wxli70@ustc.edu.cn

摘要: 氢气活化在过渡金属氧化物催化的加氢反应中起到至关重要的作用. 二氧化铈(CeO_2)表面上氢气如何活化是乙炔加氢反应中的重要科学问题. 本文利用密度泛函理论计算(DFT)的方法,系统研究了化学计量及有氧缺陷的 CeO_2(111)、(110)和(100)表面上氢气活化机理. 氢气在化学计量的 CeO_2 表面解离时仅形成羟基,而氧空位的存在可以有效促进氢气活化. CeO_{2-x}(111)和(100)缺陷表面上 H^+和 H^-物种可以共存,而在 CeO_{2-x}(110)缺陷表面上只能观察到 H^+物种. 化学计量及有氧缺陷的 CeO_2 表面上氢气活化的结构敏感性与 H^+和 H^-吸附能有关,并由氧空位形成能以及 Ce、O 离子的电荷分布决定. 该理论工作深入理解了二氧化铈基催化剂上氢气活化过程,为优化和设计高效加氢催化剂提供了理论支撑.

关键词: 二氧化铈; 氢气活化; 表面敏感性; 密度泛函理论